Antibody-functionalized polymer-coated gold nanoparticles targeting cancer cells: an in vitro and in vivo study

Marega, R.; Karmani, L.; Flamant, L.; Nageswaran, P.G.; Valembois, V.; Masereel, B.; Feron, O.; Vander Borght, T.; Lucas, S.; Michiels, C.; Gallez, B.; Bonifazi, D.

Published in:
Journal of Materials Chemistry

DOI:
10.1039/c2jm33482h

Publication date:
2012

Document Version
Publisher's PDF, also known as Version of record

Journal of Materials Chemistry

Cite this: *J. Mater. Chem.*, 2012, **22**, 21305

www.rsc.org/materials

PAPER

Antibody-functionalized polymer-coated gold nanoparticles targeting cancer cells: an *in vitro* and *in vivo* study

Riccardo Marega,†[a] Linda Karmani,†[b] Lionel Flamant,†[c] Praveen Ganesh Nageswaran,[a] Vanessa Valembois,[d] Bernard Masereel,[e] Olivier Feron,[f] Thierry Vander Borght,[f] Stephane Lucas,*[d] Carine Michiels,*[c] Bernard Gallez*[b] and Davide Bonifazi*[ag]

Received 30th May 2012, Accepted 29th July 2012
DOI: 10.1039/c2jm33482h

Gold nanoparticles (~5 nm) coated with plasma-polymerized allylamine were produced through plasma vapor deposition and bioconjugated with a monoclonal antibody targeting the epidermal growth factor receptor. The resulting nanoconjugates displayed an antibody loading of about 1.7 nmol mg^{-1} and efficiently target epidermal growth factor receptor overexpressing cell lines, as ascertained by ELISA and Western blot assays. The *in vitro* targeting properties were also confirmed *in vivo*, where a similar biodistribution profile of what was experienced for the unconjugated antibody was observed. Thanks to the possibility of doping the gold nanoparticles with radionuclides during plasma vapor deposition, the proposed functionalization strategy represents a very suitable platform for the *in vivo* cancer targeting with nanosized multifunctional particles.

Introduction

Among the different technological fields, gold nanostructures such as particles,[1] rods,[2] nanoshells[3] and nanocubes[4] have thoroughly been investigated for biomedical purposes.[5,6] In fact, thanks to their tuneable size, shape and optical absorption properties,[5,7] along with good biocompatibility profiles,[8] these nanomaterials have been proposed as sensors,[9] imaging[10] and drug-delivery platforms.[11–13] Most of these applications require surface modification of Au nanostructures, which can be easily done either through adsorption of (bio)molecules bearing thiol or amino functional groups,[14] or by polymer coating.[15] In some instances, the resulting nanomaterials showed improved water dispersability/solubility properties, therefore the assessment of the interaction of such functional nanostructures with living systems is of paramount importance for both biological properties and safety evaluation.[13] Both the assessment of biodistribution profiles and toxicity of naked or functionalized gold nanostructures has become a field of intensive research,[16] as recently summarized in an excellent review by Khlebtsov and Dykman.[17] It is clear that the biodistribution profiles depend on several factors, such as particle shape, size and surface coating properties, each one affecting the resulting pharmacokinetic profile.[17] One of the major fields of research for application of gold nanoparticles (AuNPs) is cancer treatment, where a selective accumulation of (multi)functional nanomaterials in the tumor is desired. In this respect, several reports about nanoparticle surface modifications aimed at cancer targeting have been reported in the last few years,[18] among others, those describing antibody-coupling represent a major interest.[19,20] In particular, antibodies (Abs) targeting the epidermal growth factor receptor (EGFR),[21] a membrane protein overexpressed in several kinds of solid tumors, have been conjugated to AuNPs and efficiently employed for imaging,[19,22] photothermal treatment[23] and drug delivery.[12,24] Additionally, it has been shown that this "nanoconjugation" uniformly enhances the antibody-induced EGFR endocytosis for several cancer cell lines.[25] Aiming at maximizing the cancer uptake of such nanoconjugates, it is of great importance to determine the biodistribution of antibody-functionalized AuNPs (AuNPs-Ab) in murine models

[a]*Namur Research College (NARC) and Department of Chemistry, University of Namur (FUNDP), Rue de Bruxelles 61, 5000 Namur, Belgium. E-mail: davide.bonifazi@fundp.ac.be*
[b]*Biomedical Magnetic Resonance Unit (REMA), Louvain Drug Research Institute, University of Louvain (UCL), Place de l' Université 1, 1348 Louvain-la-Neuve, Belgium. E-mail: bernard.gallez@uclouvain.be*
[c]*Unité de Recherche en Biologie Cellulaire (URBC), Namur Research Institute for LIfe Sciences (NARILIS), University of Namur (FUNDP), Rue de Bruxelles 61, 5000 Namur, Belgium. E-mail: carine.michiels@fundp.ac.be*
[d]*Research Centre for the Physics of Matter and Radiation (PMR-LARN), Namur Research Institute for LIfe Sciences (NARILIS), University of Namur (FUNDP), Rue de Bruxelles 61, 5000 Namur, Belgium. E-mail: stephane.lucas@fundp.ac.be*
[e]*Department of Pharmacy, Namur Medicine & Drug Innovation (NAMEDIC), Namur Research Institute for LIfe Sciences (NARILIS), University of Namur (FUNDP), Rue de Bruxelles 61, 5000 Namur, Belgium. E-mail: bernard.masereel@fundp.ac.be*
[f]*Institut de Recherche Expérimentale et Clinique (IREC), University of Louvain (UCL), Place de l'Université 1, 1348 Louvain-la-Neuve, Belgium. E-mail: olivier.feron@uclouvain.be; thierry.vanderborght@uclouvain.be*
[g]*Department of Chemical and Pharmaceutical Sciences, University of Trieste, Piazzale Europa 1, Trieste, 34127, Italy*
† These authors equally contributed to this work.

xenografted with human cancers. Thus, in the present work, we took advantage of the amino functionalities exohedrally exposed on relatively small sized (~5 nm) polymer-coated AuNPs (AuNPs-PPAA), synthesized through simultaneous plasma vapor deposition of Au (core) and allylamine (which leads to a plasma-polymerized-allylamine shell, PPAA),[26] to covalently immobilize *via* an amide linkage an EGFR-targeting Ab Cetuximab,[27] either in its native or ^{125}I-radiolabelled form. The resulting nanoconjugates have been thus tested to assess EGFR targeting both *in vitro* and *in vivo* murine models. *In vitro* studies showed the preferential binding of the nanoconjugate to EGFR overexpressing cancer cells (A431), with very low aspecific binding to EGFR non expressing cell lines (CHO and EAhy926), and the blocking of the EGF-induced biochemical effects, as assessed through Western blot analysis. *In vivo* results showed that tumor uptake was not significantly different between free and nanoconjugated Cetuximab, highlighting the preservation of antibody recognition after the bioconjugation step.

Results and discussion

AuNPs-PPAA synthesis and bioconjugation with Ab and Ab-^{125}I

Fig. 1 reports the synthetic pathway toward the preparation of the bioconjugates between **AuNPs-PPAA** and purified Cetuximab, either in its native (Ab) or ^{125}I-bearing form (**Ab-^{125}I**), generating **AuNPs-PPAA-Ab** and **AuNPs-PPAA-Ab-^{125}I**, respectively. The amino groups present in the polymeric shell of **AuNPs-PPAA** were exploited for amide bond formation with carboxyl groups located on Cetuximab, through carbodiimide chemistry in buffer solution (Fig. 1a). By repeating the same reaction, but without the use of the carbodiimide, a physical mixture between **AuNPs-PPAA** and Cetuximab (**AuNPs-PPAA/Ab**) was also prepared, as a reference compound (Fig. 1b).

To determine both morphology and size distribution of the pristine nanostructures, **AuNPs-PPAA** were directly deposited onto a TEM grid, revealing the presence of spherical objects with an average size between 3 and 5 nm (Fig. 2a). After a diafiltration step, necessary to remove excess, unbound PPAA left from PVD cycles, spherical objects with diameters ranging from 3 to 15 nm (mean = 4.83 ± 1.69 nm, Fig. 2b), as a consequence of occasional AuNPs agglomeration induced by the diafiltration process, were clearly detected by TEM imaging. Diafiltered samples containing

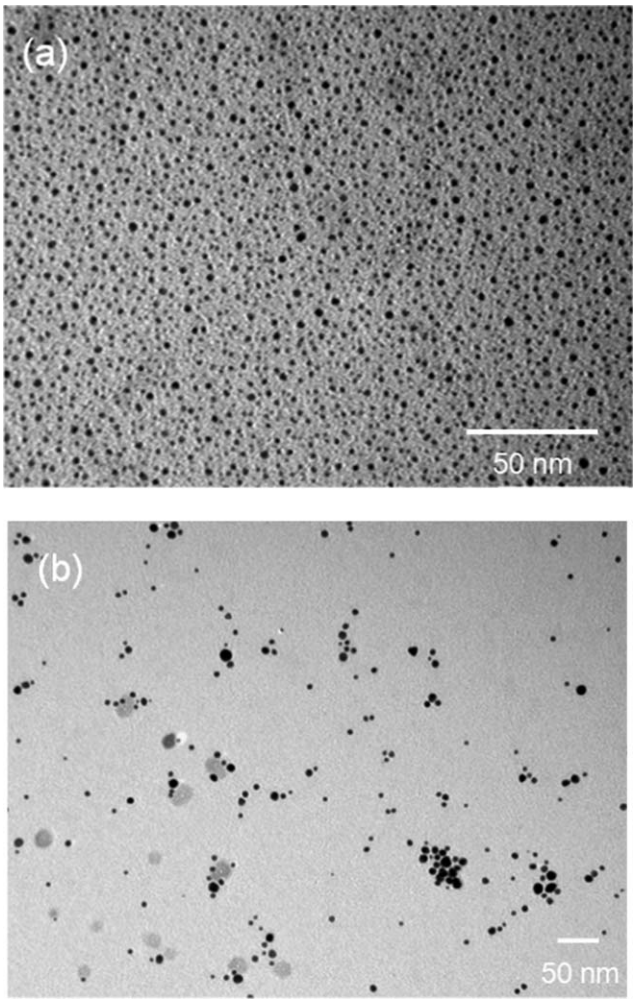

Fig. 2 Bright-field TEM images of **AuNPs-PPAA** on Cu grids: (a) as produced and (b) after dispersion and diafiltration.

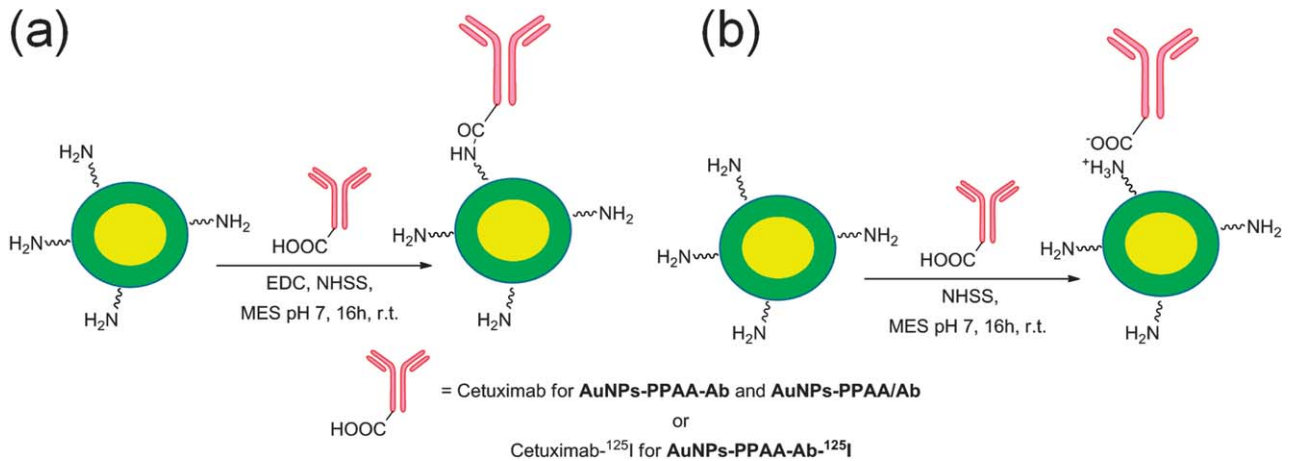

Fig. 1 Synthetic pathway for the synthesis of covalent **AuNPs-PPAA-Ab** (a) and physiadsorbed **AuNPs-PPAA/Ab** bioconjugates (b). Yellow: AuNPs, green: PPAA coating. EDC = 1-Ethyl-3(3-dimethylaminopropyl)carbodiimide hydrochloride, NHSS = *N*-Hydroxysulfosuccinimide sodium salt and MES = 2-(*N*-morpholino)ethanesulfonic acid.

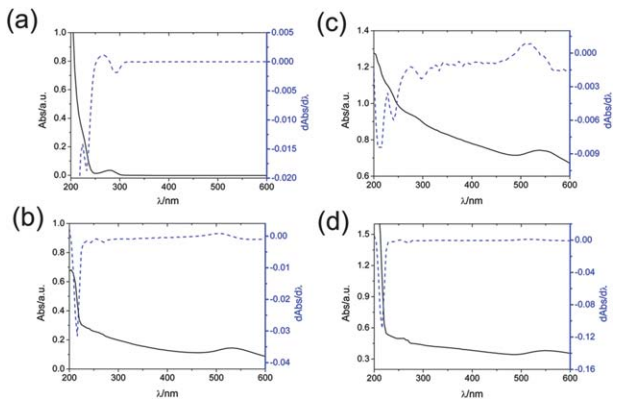

Fig. 3 Steady-state UV-Vis absorption spectra (——) and derivative plots (dAbs/dλ, **---**) for Ab (a), **AuNPs-PPAA** (b), **AuNPs-PPAA-Ab** (c) and **AuNPs-PPAA/Ab** (d).

AuNPs-PPAA-Ab, **AuNPs-PPAA/Ab** and reference starting materials (*i.e.*, AuNPs and Ab) were first analyzed by steady-state UV-Vis spectroscopy (Fig. 3). The absorption spectrum of Cetuximab shows the typical proteinic signature at 280 nm, which belongs to the aromatic groups-bearing aminoacidic residues (*i.e.*, phenylalanine, tyrosine, tryptophane and histidine), and the peptidic feature at 220 nm, as also clearly displayed in the dAbs/dλ plot (Fig. 3a). On the other hand, the **AuNPs-PPAA** absorption spectrum shows a surface plasmon absorption feature at 530 nm, characteristic of small-sized AuNPs,[7] and then a steady absorbance increase towards the UV region, the latter providing a characteristic peak centered at 208 nm in the dAbs/dλ plot (Fig. 3b). The dAbs/dλ plot for samples containing **AuNPs-PPAA-Ab** clearly shows a very good overlap with both Cetuximab- and **AuNPs-PPAA**-centered signatures (Fig. 3c), suggesting the simultaneous presence of the two moieties in the bioconjugate and thus their covalent linkage.

In contrast, the dAbs/dλ plot for **AuNPs-PPAA/Ab** only shows the presence of the **AuNPs-PPAA**-centered features (Fig. 3d), thus suggesting the efficient elimination of the non-covalently linked Ab counterpart by discontinuous diafiltration.

To evaluate **AuNPs-PPAA-Ab** composition, thermogravimetric analysis under inert atmosphere was carried out (Fig. 4). Under these conditions we expected to determine the pyrolytic behaviour of the single components (Ab, PPAA and AuNPs) constituting the bioconjugate **AuNPs-PPAA-Ab**. PPAA (Fig. 4a) showed a main pyrolysis event in the range between 100 and 500 °C, with a weight loss at 600 °C of 30.53 wt%. **AuNPs-PPAA** also showed a main pyrolysis occurring between 100 and 500 °C, with a weight loss at 600 °C of 25.30 wt% (Fig. 4b). Since Au has a high thermal stability (melting point at about 1060 °C), we can assume that the observed weight loss in **AuNPs-PPAA** is due to the decomposition of the PPAA layer, allowing for compositional estimation that gives 17.13 and 82.87 wt% for Au and PPAA, respectively. By looking at Ab pyrolysis behaviour (Fig. 4c), there is also a weight loss in the range between 100 and 500 °C, with a clear maximum at about 300 °C (Ab decomposition thermal signature) and a related weight loss of 74.92 wt% at 600 °C.

AuNPs-PPAA-Ab conjugate plots (Fig. 4d) showed the thermal signature of Ab decomposition at about 300 °C, further suggesting that the Ab coupling has occurred, and an increased weight loss of 19.23 wt% compared to **AuNPs-PPAA**. Considering the residual weights observed for each compound at 600 °C (74.70 wt% for **AuNPs-PPAA**, 25.08 wt% for Ab) and the additional weight loss after Ab immobilization, it is possible to estimate the **AuNPs-PPAA-Ab** composition, which was 12.73 wt% for Au, 61.60 wt% for PPAA and 25.67 wt% for Ab (*i.e.*, about 1.7 nmols of Ab per mg of material).

For the preparation of **AuNPs-PPAA-Ab-^{125}I** a known radiolabeling procedure based on the Iodo-Gen method was employed. The radioiodination yield for Ab was typically 70–80%, whereas the radiochemical purity immediately after purification was greater than 99%. The resulting specific activity was 7.4 kBq per μg Ab. The ^{125}I-to-Ab ratio was about 0.014, which means that roughly one out of seventy Ab carries one ^{125}I atom. Samples were stored several days at 4 °C and analyzed for overall *in vitro* stability. The amount of free iodide in purified **Ab-^{125}I** remained below 2% even after 25 days at 4 °C.

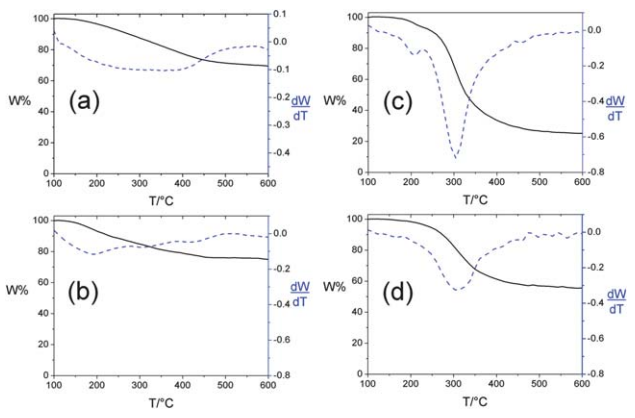

Fig. 4 Temperature-modulated (——) and derivative (d*W*/d*T*, **---**) plots of PPAA (a), **AuNPs-PPAA** (b), Ab (c) and **AuNPs-PPAA-Ab** (d), recorded under N_2 atmosphere.

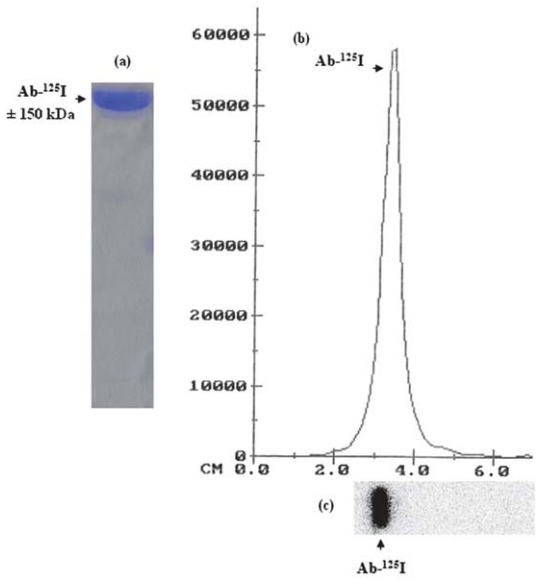

Fig. 5 Electrophoresis gel profile of **Ab-^{125}I** using SDS-PAGE 8% under non-reducing conditions (a). The migration gel was scanned by a Bioscan (b) and Phosphor Imager (c).

Table 1 Measured radioactivity of aliquots (1 mL) of the conjugate at various time intervals

t (h)	Measured activity[a] ($csec^{-1}$)	V_{tot} (mL)	Activity ($csec^{-1}$)
t_0	133	6.4	851
t_{1h}	85.4	9.4	803
t_{24h}	11.8	9.4	111
t_{Final}	24.7	5.0	125

[a] As the purification through diafiltration proceeded, a reduction of radioactivity due to **Ab-^{125}I** elimination occurred, until a steady value of radioactivity (t_{Final}), consistent with partial **Ab-^{125}I** immobilization, was assessed.

Electrophoresis of **Ab-^{125}I** under non-reducing conditions followed by autoradiography showed the 150 kDa Ab band and a single peak of radioactivity (Fig. 5), which means that antibody integrity remained preserved after the labelling procedure.

The conjugation reaction between **AuNPs-PPAA** and **Ab-^{125}I** was then performed under the same conditions as those employed for unlabeled Cetuximab (Fig. 1a). Reaction progress was monitored by measuring the total activity ($csec^{-1}$) of aliquots sampled at periodic intervals (Table 1), which allowed estimating an **Ab-^{125}I** immobilization efficiency of about 20%.

In vitro evaluation of EGFR targeting

At first, the relative binding affinity of **AuNPs-PPAA-Ab** toward an EGFR overexpressing cell line has been determined by a cell based ELISA study. To this aim, we have selected the A431 cell line, since these cells express high amounts of EGFR (EGFR+).[28] As a negative control, cells that do not express EGFR, Chinese hamster ovary (CHO) cells, have been selected (EGFR−). Consequently, different concentrations of Ab and of **AuNPs-PPAA-Ab** were tested both on EGFR+ and EGFR− cells (Fig. 6). As expected, Ab bound to EGFR+ cells in a concentration-dependent manner, but not to EGFR- cells. Interestingly, **AuNPs-PPAA-Ab** also bound to EGFR+ cells in a concentration-dependent way, suggesting the retention of the correct Ab conformation for the epitope selection and interaction in **AuNPs-PPAA-Ab** conjugates. A very slight unspecific binding of **AuNPs-PPAA-Ab** to EGFR− cells was also observed. Similar results were obtained for another EGFR− cell line, EAhy926 endothelial cells (data not shown).

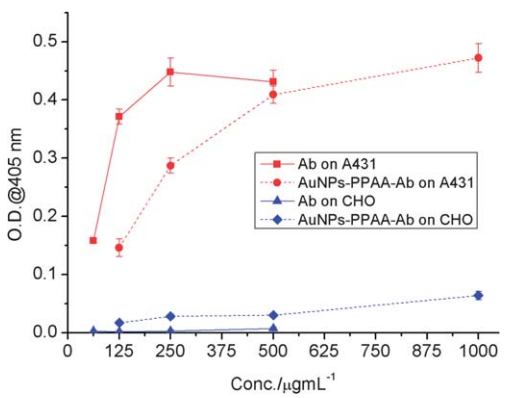

Fig. 6 Surface ELISA for Ab and **AuNPs-PPAA-Ab** on EGFR+ (A431) and EGFR− (CHO) cells. Different concentrations of Ab and of **AuNPs-PPAA-Ab** were tested. The concentrations are expressed as μg of Ab per mL. Results are presented as means ± 1 S.D ($n = 4$).

From the concentration-dependent ELISA outcomes, binding affinity toward A431 cells was quantified. Half maximal effective concentration (EC_{50}) for Ab was estimated as 0.08 μg mL^{-1}, while the EC_{50} for **AuNPs-PPAA-Ab** was 0.19 μg mL^{-1}. For the same number of antibody molecules, the spatial distribution is constrained around NPs for NP-coupled Ab in comparison to free Ab so that not all the Ab molecules are available to recognize the antigen that is distributed on the monolayer cell surface. This could explain the apparent lower affinity of the Ab when coupled to the NPs.

We then determined the capability to inhibit the EGF-induced phosphorylation of EGFR (at tyrosine 1173) through phosphorylation assays and subsequent Western Blot Analysis. Serum-starved cells (24 hours) were incubated with or without Ab or **AuNPs-PPAA-Ab** for 7 minutes before being stimulated or not with 10 ng mL^{-1} EGF for 10 minutes. As expected EGF stimulates EGFR phosphorylation, an effect that was inhibited if cells were pre-incubated with Ab. Negative results were obtained for both CHO and EAhy926 cells (EGFR−). Fig. 7 shows that such a competition was also observed in the presence of **AuNPs-PPAA-Ab**. All these binding results shows that, although slightly reduced compared to Cetuximab alone, the Ab affinity after immobilization onto **AuNPs-PPAA** is qualitatively preserved.

In vivo assessment of EGFR targeting

EGFR targeting was studied in NMRI nude mice bearing A431 epidermoid carcinoma tumors. Comparative pharmacokinetic

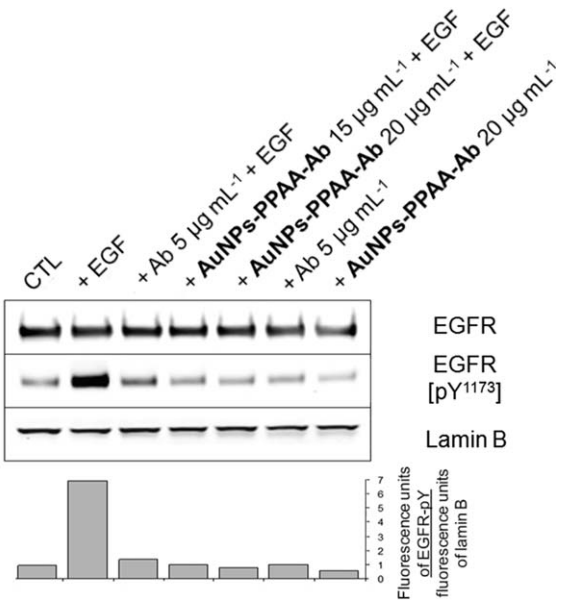

Fig. 7 Inhibition of EGF-induced phosphorylation of EGF receptors by Ab or **AuNPs-PPAA-Ab**. A431 cells were incubated with Ab or **Au-NPs-PPAA-Ab** for 7 min before being stimulated with 10 ng mL^{-1} EGF for 10 min. Lysates were separated by electrophoresis and analyzed by Western blotting using anti-EGFR or anti-phospho-EGF receptor (Tyr1173) antibodies. Lamin B was used as the loading control. The ratio between fluorescent intensity of the bands corresponding to phospho-EGFR and to Lamin B was calculated for each lane.

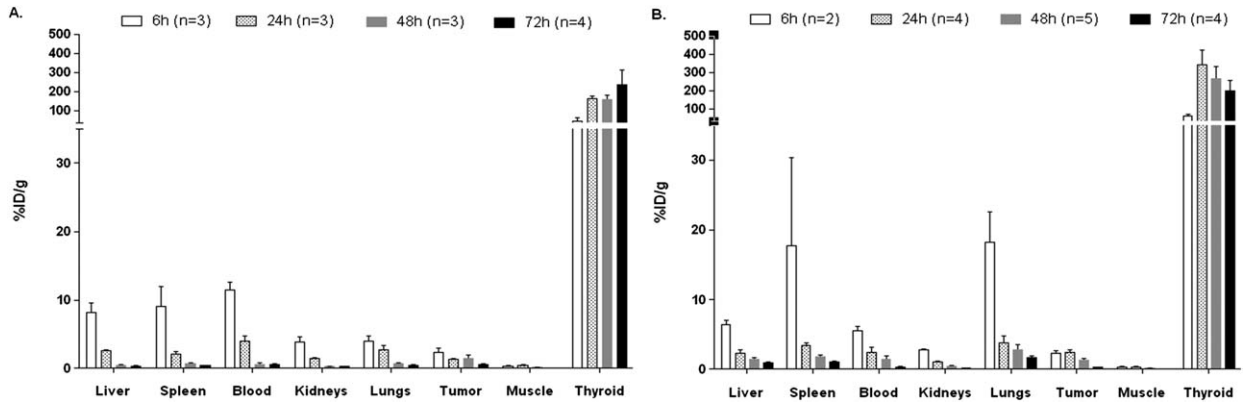

Fig. 8 Biodistribution of 60 kBq of **Ab-^{125}I** (A) or **AuNPs-PPAA-Ab-^{125}I** (B) (13.5–16 μg) in nude mice bearing A431 tumors at 6, 24, 48 and 72 h after injection. Columns, mean %ID per g normal tissue and tumor; bars, SEM (n = 2–5).

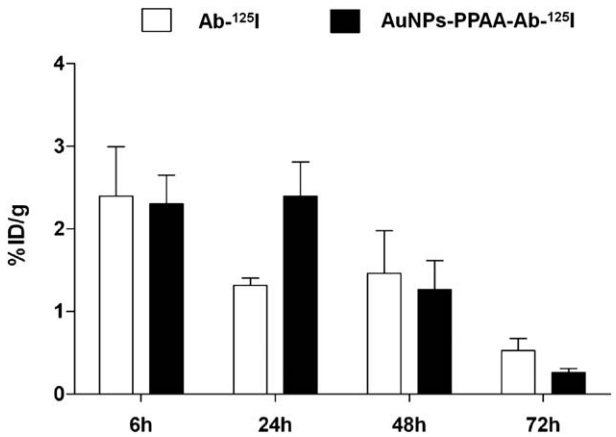

Fig. 9 Tumor uptake of 60 kBq of **Ab-^{125}I** or **AuNPs-PPAA-Ab-^{125}I** (13.5–16 μg) in nude mice bearing A431 tumors at 6, 24, 48 and 72 h after injection. Columns, mean; bars, SEM (n = 2–5).

assessment of both **Ab-^{125}I** and **AuNPs-PPAA-Ab-^{125}I** was evaluated by *ex vivo* biodistribution studies. The biodistribution data are presented in Fig. 8. At each time post-injection, radioactivity uptake levels in tumors were not significantly different between the conjugates (Fig. 9). The highest tumor-to-blood ratio was observed after 48 h for both groups and was respectively 2.38 ± 0.18 for **Ab-^{125}I** and 1.10 ± 0.42 for **AuNPs-PPAA-Ab-^{125}I**.

Tumor-to-blood ratios were not significantly different between the two groups except at 6 h post-injection (Fig. 10). This difference can be explained by the blood pool activity that is significantly different between the two groups at early time. The most remarkable differences between both biodistribution patterns were observed for uptake in lungs, spleen and liver. At 6 h pi., lungs and spleen uptake levels were 3.98 ± 0.83 and 9.13 ± 2.91 for **Ab-^{125}I**, and 18.25 ± 4.34 and 17.80 ± 12.64 for **AuNPs-PPAA-Ab-^{125}I**, respectively. For liver, these values were 8.18 ± 1.39 and 6.42 ± 0.61 for **Ab-^{125}I** and **AuNPs-Ab-^{125}I**, respectively. Uptake levels in kidneys, thyroid and skeletal muscles were similar for both radioimmunoconjugates. The reticuloendothelial system uptake is more important for **AuNPs-PPAA-Ab-^{125}I** than **Ab-^{125}I**. This may explain the lower blood activity at early times. For all normal tissues (liver, spleen, kidneys, lungs and muscles), there is no specific uptake or accumulation of **AuNPs-PPAA-Ab-^{125}I** compared to the control group. The radioactivity level decreased over time.

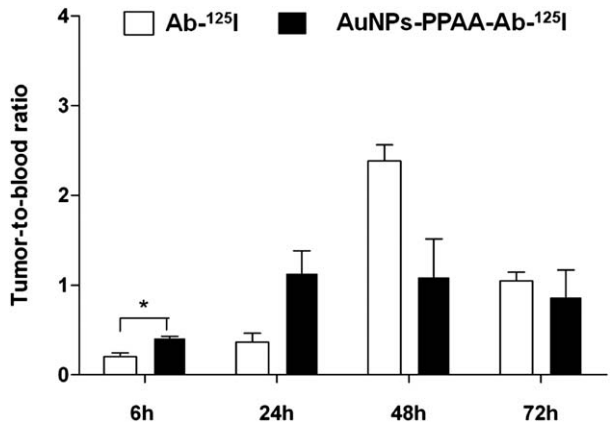

Fig. 10 Tumor to blood ratios of 60 kBq of **Ab-^{125}I** or **AuNPs-PPAA-Ab-^{125}I** (13.5–16 μg) in nude mice bearing A431 tumors at 6, 24, 48 and 72 h after injection. Columns mean; bars, SEM (n = 2–5). *P < 0.05, significant differences between **Ab-^{125}I** and **AuNPs-Ab-^{125}I**.

Very interestingly, despite the small decrease in binding capacity of **AuNPs-PPAA-Ab-^{125}I** to the EGFR target, tumor uptake was not significantly different between the two groups. Data thus indicate that coupling nanoparticles to Cetuximab does not seem to affect the pharmacokinetic behaviour of the antibody, and particularly the tumor uptake. Therefore, an antibody conjugated to gold nanoparticles seems to maintain its targeting activity towards EGFR over-expressed on tumor cells. Nonetheless, the high thyroid uptake means an *in vivo* deiodination related to the degradation of **Ab-^{125}I**, which induces a rapid free iodine clearance and a low tumor contrast expressed as a tumor-to-blood ratio.[29] This chemical instability may lead to errors in the estimation of the actual antibody tumor uptake.

Conclusions

Polymer-coated AuNPs have been efficiently produced by plasma vapor deposition, through an automated batch wise procedure, and subsequently covalently decorated with native or radioiodinated Cetuximab through amide bond formation reaction. The resulting bioconjugates selectively target EGFR

overexpressing cell lines, allowing for the *in vitro* binding of cancer-like cells, as evaluated by ELISA and Western blot analysis after phosphorylation studies. Although the occurrence of the parasite deiodination of the radiolabeled Cetuximab, as detected by high thyroid uptake, certainly affects (*i.e.*, underestimating the observed value) the quantification of the accumulation in the tumor tissues, the bioconjugates showed an *in vivo* pharmacokinetic profile very similar to that of the uncoupled Ab, thus supporting our idea that such nanostructures are suitable scaffolds to be implemented for *in vivo* treatments. In particular, the possibility of further doping the AuNPs core with radioactive species during the PVD synthesis opens the way toward the development of a new generation of radioactive bioconjugates possibly displaying a theranostic activity.

Experimental part

Materials

All chemicals were purchased from commercial sources and used without further purification. 1-Ethyl-3-(dimethylaminopropyl)-3-carbodiimide hydrochloride (EDC·HCl), *N*-hydroxy-sulphosuccinimide sodium salt (NHSS) and 2-(*N*-morpholino)ethanesulphonic acid hydrate (MES) were obtained from Sigma-Aldrich and used without further purification. Allylamine was obtained from Sigma-Aldrich. Water was purified using a Millipore Milli-Q water production system. Commercially available Cetuximab formulation (Erbitux® 2 or 5 mg mL^{-1}, Merck & Co.) was purified by discontinuous diafiltration in centrifugal concentrators with a molecular weight cut-off (MWCO) of 10 000 g mol^{-1} (Sartorius Vivaspin) and the purified antibody was isolated by freeze-drying (Ab). Iodo-Gen kit was obtained from Pierce Thermo scientific. ^{125}I was purchased from Best Medical Belgium and radiolabeled antibodies were purified on a Sephadex G-25 column (GE Healthcare Europe).

Characterizations

Transmission electron microscopy (TEM) images were acquired with a Philips Tecnai 10 transmission electron microscope (TEM) operating at 80 keV and in bright-field mode. Samples for TEM analysis were obtained by depositing onto carbon-coated Cu grids directly during PVD process (Fig. 2a) or by using suitable solutions of **AuNPs-PPAA** in H_2O (Fig 2b). All the thermogravimetric analyses were performed with a *TGA Q500* instrument manufactured by TA instruments (Italy), under a N_2 flow of 60 mL min^{-1} and with the following method: equilibration from room temperature to 100 °C, isothermal heating at 100 °C for 20 min, then ramp from 100 °C to 1000 °C (heating rate of 10 °C min^{-1}). UV-Vis spectra were recorded on a Cary 5000 Spectrophotometer (*Varian*), using 1 cm path quartz or optical glass cuvettes. Quality controls of radiolabeled antibodies were performed by paper chromatography, Bioscan analysis (Bioscan system 200 imaging scanner), SDS-PAGE electrophoresis and by gel scanning through a Phosphor Imager (Fujifilm FLA-5100). The amount of radioactivity in tumors, blood and organs (liver, spleen, kidneys, lung, skeletal muscles and thyroid) was measured in a gamma well counter (1480 Wallac Wizard 3″ automatic γ-counter; Perkin Elmer, Inc.).

Synthesis of AuNPs-PPAA and antibody conjugation

Synthesis of gold nanoparticles coated with plasma-polymerized allylamine (**AuNPs-PPAA**) by plasma vapor deposition (PVD) was already reported.[26] The resulting NaCl embedded nanoparticles were then dispersed in acetate buffer (pH = 5) under 5 min of sonication and then purified from the PPAA and NaCl excess by discontinuous diafiltration in centrifugal concentrators with a molecular weight cut-off (MWCO) of 10 000 g mol^{-1}. Ab (5 mg) was dissolved in 10 mL of 0.1 M MES buffer (190 mg in 10 mL H_2O, pH = 7), and then a solution of EDC·HCl (2 mg, 0.01 mmol) and NHSS (2 mg, 0.01 mmol) in 10 mL of 0.1 M MES buffer was added. The resulting mixture was stirred at 25 °C for 15 min, after that a solution of **AuNPs-PPAA** (0.65 mg mL^{-1}, 8.0 mL, 5.2 mg) in H_2O was added. The reaction was stirred at 25 °C for 16 hours, after which it was purified by discontinuous diafiltration against H_2O in centrifugal concentrators with MWCO of 300 000 g mol^{-1}. Purification was completed when the electrical conductivity of the filtrate was almost equal to that of H_2O. **AuNPs-PPAA-Ab** were isolated through freeze-drying, affording a pinkish red powder (6.5 mg).

Radioiodination of Cetuximab

Ab radioiodination with ^{125}I was done using the Iodo-Gen method as described in instructions of use by Pierce. In brief, a mixture of sodium iodide (3700 MBq mL^{-1}) and Cetuximab (20 mg mL^{-1}) dissolved in 0.01 M sodium phosphate buffered saline (NaCl 0.14 M, pH 7.4) was added to an Iodo-Gen-coated reaction vial (50 μg iodogen coating the inner surface of a 100 μL vial) and reacted for 5 min at room temperature with stirring every 30 seconds. Protein-bound iodine was separated from free iodide by passing over a Sephadex G-25 column equilibrated with PBS 0.01 M pH 7.4. Quality control of radiolabeled Ab (**Ab-^{125}I**) was performed by using paper chromatography (eluent: MeOH–H_2O, 70 : 30, v/v) followed by Bioscan analysis to determine the radiochemical yield and purity. In addition, **Ab-^{125}I** integrity was checked by SDS-PAGE (8%, under non-reducing conditions) and analyzed by a Bioscan and Phosphor Imager.

Synthesis of AuNPs-PPAA-Ab-^{125}I

2 mg of **Ab-^{125}I** were redissolved in 5 mL of 0.1 M MES buffer and treated with a solution of EDC·HCl (1 mg, 0.005 mmol) and NHSS (1 mg, 0.005 mmol) in 5 mL of 0.1 M MES buffer. The mixture was stirred for 15 min at 25 °C, after which a solution of **AuNPs-PPAA** (0.65 mg mL^{-1}, 2.0 mL, 1.30 mg) in H_2O was added. The reaction was stirred at 25 °C for a period of 16 hours after which it was purified by diafiltration using a membrane filter of molecular weight cut-off 300 000 g mol^{-1}. The purification was completed when the electrical conductivity of the filtrate was almost equal to that of H_2O. The retentate was finally redissolved in 3.0 mL of deionized H_2O by sonication affording a H_2O solution of **AuNPs-PPAA-Ab-^{125}I**.

Cell culture

Human epithelial carcinoma cells A431 and Chinese hamster ovary cells CHO were maintained in culture in 75 cm^2

polystyrene flasks (Corning) with respectively 15 mL of Dulbecco's modified Eagle's medium (DMEM) or Roswell Park Memorial Institute medium (RPMI 1640, Invitrogen), containing 10% of fetal calf serum (Invitrogen) and incubated under an atmosphere containing 5% CO_2.

Surface ELISA

A431 or CHO cells (10^5 per well) were grown in 96 well plates (Costar) 24 hours prior to the ELISA test. Cells were rinsed once with PBS and then fixed 10 min with PBS containing 4% paraformaldehyde. After one wash with PBS, wells were blocked with 5% of non-fat dry milk in PBS for 1 hour at room temperature. Cells were rinsed one time with PBS and one time with BSA 1% in PBS for 5 min. Ab or **AuNPs-PPAA-Ab** were added to the cells at various concentrations for 1 hour at room temperature. Plates were washed three times with PBS–BSA, and a mouse monoclonal anti-human IgG–biotin antibody (Sigma) diluted in PBS–BSA at 1 μg mL^{-1} was added for 1 hour at room temperature. Cells were washed three times and incubated with streptavidin-alkaline phosphatase (Sigma) for 30 min at room temperature. After three washing steps with PBS–BSA and one with PBS, alkaline phosphatase activity was revealed with 1 mg mL^{-1} *p*-nitrophenylphosphate in 0.1 M diethanolamine pH 10.3 containing 1.5 mM levamisole hydrochloride. The reaction was stopped with NaOH 2 N and the surface expression was quantified spectrophotometrically, reading the optical density (405 nm) 45 min after addition of the substrate.

Phosphorylation studies

A431 cells were grown to 90% confluence in complete medium in T75 flasks, and they were starved in DMEM with 0.5% BSA (Sigma) for 24 hours prior to stimulation. Cells were incubated for 7 min with Ab or **AuNPs-PPAA-Ab** and then stimulated with 10 ng mL^{-1} EGF (R&D Systems) for 10 min at 37 °C. Following stimulation, cells were washed with ice-cold PBS containing 1 mM sodium orthovanadate. Cells were lysed with a lysis buffer (Tris 20 mM pH 7.5, NaCl 150 mM, EDTA 1 mM, EGTA 1 mM, sodium deoxycholate 1%, Nonidet P40 1%, glycerol 10%) containing a protease inhibitor mixture («Complete» from Roche Molecular Biochemicals, 1 tablet in 2 mL H_2O, added at a 1 : 25 dilution) and phosphatase inhibitors ($NaVO_3$ 25 mM, PNPP 250 mM, α-glycerophosphate 250 mM and NaF 125 mM, at a 1 : 25 dilution). Protein concentration in cell lysates was evaluated by Bradford protein assay (Bio-rad) and 15 μg proteins were separated by electrophoresis on a 3–8% Tris–acetate gel (NuPage, Invitrogen). After semi-dry transfer onto a low IR background PVDF (polyvinylidene fluoride) membrane (Millipore) for 2 h at 1 mA cm^2, the membrane was left for 2 h in Licor blocking agent 2× diluted in PBS before incubation during 2 h with the primary antibody diluted in Odyssey blocking buffer (Licor) containing 0.1% Tween 20 (Sigma). The membrane was washed 4 × 5 min with PBS-Tween 0.1%, incubated 1 h with infrared dye specific secondary antibodies (Licor) diluted in Odyssey + Tween 0.1% and washed 4 × 5 min with PBS-Tween 0.1% and 2 × 5 min with PBS before protein detection using the Odyssey Infrared Imaging System (Licor). Fluorescence Western blot analysis by infrared technology (Licor) allows the quantification of the fluorescent intensity of the bands corresponding to the protein of interest. Western blotting analysis was performed by infrared fluorescence with rabbit anti-phospho-EGF receptor (Tyr1173) monoclonal antibody (# 4407 Cell Signaling) used at 1/1000 dilution or rabbit anti-EGF receptor monoclonal antibody (# 4267 Cell Signaling) used at 1/5000 dilution. Goat anti-lamin B antibody (SC-6212 Santa Cruz) (final dilution 1/2000) was used for normalization. Rabbit or goat IgG infrared dye-linked antibody (Licor) was used at 1/10 000 dilution as a secondary antibody.

Comparative biodistribution studies in mice

NMRI nude mice (athymic nu/nu, 29–36 g, Janvier, France) were 5–8 weeks old at the time of the experiments. The human epidermoid carcinoma cell line A431 (10×10^6) was injected subcutaneously into the flank of each mouse. Biodistribution studies were performed when tumors reached a size of approximately 7.5–8.5 mm. All animal experiments were approved by the local ethics committee for animal research in compliance with the principles of laboratory animal care. Two groups of mice were injected i.v. into the lateral tail vein with either a mixture of 74 kBq **Ab-^{125}I** (control group) or with **AuNPs-PPAA-Ab-^{125}I** (total of 13.5 to 16 μg of Ab per mouse). Typically, groups of 2–5 mice per time point (6, 24, 48 and 72 h after injection) were anesthetized, weighed, killed by cervical dislocation and dissected. Radioactivity uptake was expressed as the percentage of injected dose per gram of tissue (%ID g^{-1}) and as tumor-to-blood ratios. The results were expressed as the mean ± SEM. Data calculations were performed with Prism software (GraphPad Software Inc.). The differences in tissue uptake between the two groups were considered significant if the *P* values from unpaired *t* tests were less than 0.05.

Acknowledgements

This work was supported by the Région Wallonne through the "TARGAN" project, the FRS-FNRS, (FRFC contracts no. 2.4.550.09 and 2.4.617.07.F and MIS no. F.4.505.10.F), Associazione Italiana Ricerca sul Cancro (AIRC), the "Loterie Nationale", the "TINTIN" ARC project (09/14-023) and the University of Namur (internal funding). R.M. thanks FRS-FNRS for his post-doctoral fellowship. The authors thank Dr Chiara Fabbro for the TGA measurements at the University of Trieste.

Notes and references

1 R. L. Whetten, J. T. Khoury, M. M. Alvarez, S. Murthy, I. Vezmar, Z. L. Wang, P. W. Stephens, C. L. Cleveland, W. D. Luedtke and U. Landman, *Adv. Mater.*, 1996, **8**, 428; S. Chen, R. S. Ingram, M. J. Hostetler, J. J. Pietron, R. W. Murray, T. G. Schaaff, J. T. Khoury, M. M. Alvarez and R. L. Whetten, *Science*, 1998, **280**, 2098; M. C. Daniel and D. Astruc, *Chem. Rev.*, 2004, **104**, 293; Y. Lu and W. Chen, *Chem. Soc. Rev.*, 2012, **41**, 3594.
2 X. Huang, S. Neretina and M. A. El-Sayed, *Adv. Mater.*, 2009, **21**, 4880.
3 R. D. Averitt, D. Sarkar and N. J. Halas, *Phys. Rev. Lett.*, 1997, **78**, 4217.
4 Y. Sun and Y. Xia, *Science*, 2002, **298**, 2176.
5 M. Hu, J. Chen, Z. Y. Li, L. Au, G. V. Hartland, X. Li, M. Marquez and Y. Xia, *Chem. Soc. Rev.*, 2006, **35**, 1084.

6 R. Arvizo, R. Bhattacharya and P. Mukherjee, *Expert Opin. Drug Delivery*, 2010, **7**, 753; C. M. Cobley, J. Chen, E. C. Cho, L. V. Wang and Y. Xia, *Chem. Soc. Rev.*, 2011, **40**, 44; S. Jelveh and D. B. Chithrani, *Cancers*, 2011, **3**, 1081.
7 S. Eustis and M. A. El-Sayed, *Chem. Soc. Rev.*, 2006, **35**, 209.
8 H. J. Johnston, G. Hutchison, F. M. Christensen, S. Peters, S. Hankin and V. Stone, *Crit. Rev. Toxicol.*, 2010, **40**, 328.
9 U. H. F. Bunz and V. M. Rotello, *Angew. Chem., Int. Ed.*, 2010, **49**, 3268; K. M. Mayer and J. H. Hafner, *Chem. Rev.*, 2011, **111**, 3828; S. J. Tan, M. J. Campolongo, D. Luo and W. Cheng, *Nat. Nanotechnol.*, 2011, **6**, 268.
10 C. J. Murphy, A. M. Gole, S. E. Hunyadi, J. W. Stone, P. N. Sisco, A. Alkilany, B. E. Kinard and P. Hankins, *Chem. Commun.*, 2008, **8**, 544; E. Boisselier and D. Astruc, *Chem. Soc. Rev.*, 2009, **38**, 1759; Z. Wang and L. Ma, *Coord. Chem. Rev.*, 2009, **253**, 1607.
11 J. D. Byrne, T. Betancourt and L. Brannon-Peppas, *Adv. Drug Deliv. Rev.*, 2008, **60**, 1615.
12 P. Ghosh, G. Han, M. De, C. K. Kim and V. M. Rotello, *Adv. Drug Deliv. Rev.*, 2008, **60**, 1307.
13 R. A. Sperling, P. Rivera Gil, F. Zhang, M. Zanella and W. J. Parak, *Chem. Soc. Rev.*, 2008, **37**, 1896.
14 K. G. Thomas and P. V. Kamat, *Acc. Chem. Res.*, 2003, **36**, 888; D. A. Giljohann, D. S. Seferos, W. L. Daniel, M. D. Massich, P. C. Patel and C. A. Mirkin, *Angew. Chem., Int. Ed.*, 2010, **49**, 3280; W. R. Algar, D. E. Prasuhn, M. H. Stewart, T. L. Jennings, J. B. Blanco-Canosa, P. E. Dawson and I. L. Medintz, *Bioconj. Chem.*, 2011, **22**, 825.
15 J. Shan and H. Tenhu, *Chem. Commun.*, 2007, 4580; D. Li, Q. He and J. Li, *Adv. Colloid Interface Sci.*, 2009, **149**, 28; B. Masereel, M. Dinguizli, C. Bouzin, N. Moniotte, O. Feron, B. Gallez, T. Vander Borght, C. Michiels and S. Lucas, *J. Nanopart. Res.*, 2011, **13**, 1573.
16 G. Sonavane, K. Tomoda and K. Makino, *Colloids Surf. B*, 2008, **66**, 274; G. Zhang, Z. Yang, W. Lu, R. Zhang, Q. Huang, M. Tian, L. Li, D. Liang and C. Li, *Biomaterials*, 2009, **30**, 1928; S. K. Balasubramanian, J. Jittiwat, J. Manikandan, C. N. Ong, L. E. Yu and W. Y. Ong, *Biomaterials*, 2010, **31**, 2034; J. Lipka, M. Semmler-Behnke, R. A. Sperling, A. Wenk, S. Takenaka, C. Schleh, T. Kissel, W. J. Parak and W. G. Kreyling, *Biomaterials*, 2010, **31**, 6574; E. S. Glazer, C. Zhu, A. N. Hamir, A. Borne, C. S. Thompson and S. A. Curley, *Nanomedicine*, 2011, **5**, 459; S. Hirn, M. Semmler-Behnke, C. Schleh, A. Wenk, J. Lipka, M. Schäffler, S. Takenaka, W. Möller, G. Schmid, U. Simon and W. G. Kreyling, *Eur. J. Pharm. Biopharm.*, 2011, **77**, 407.
17 N. Khlebtsov and L. Dykman, *Chem. Soc. Rev.*, 2011, **40**, 1647.
18 X. Huang, P. K. Jain, I. H. El-Sayed and M. A. El-Sayed, *Nanomedicine*, 2007, **2**, 681; C. R. Patra, R. Bhattacharya, D. Mukhopadhyay and P. Mukherjee, *Adv. Drug Deliv. Rev.*, 2010, **62**, 346; A. Kumar, B. Mazinder Boruah and X. J. Liang, *J. Nanomater.*, 2011, **2011**, 202187; Z. Z. J. Lim, J. E. J. Li, C. T. Ng, L. Y. L. Yung and B. H. Bay, *Acta Pharmacol. Sin.*, 2011, **32**, 983; A. Llevot and D. Astruc, *Chem. Soc. Rev.*, 2012, **41**, 242.
19 I. H. El-Sayed, X. Huang and M. A. El-Sayed, *Nano Lett.*, 2005, **5**, 829.
20 E. S. Day, L. R. Bickford, J. H. Slater, N. S. Riggall, R. A. Drezek and J. L. West, *Int. J. Nanomed.*, 2010, **5**, 445; G. J. Kim, S. R. Park, G. C. Kim and J. K. Lee, *Plasma Medicine*, 2011, **1**, 45.
21 N. Normanno, A. De Luca, C. Bianco, L. Strizzi, M. Mancino, M. R. Maiello, A. Carotenuto, G. De Feo, F. Caponigro and D. S. Salomon, *Gene*, 2006, **366**, 2; C. M. Rocha-Lima, H. P. Soares, L. E. Raez and R. Singal, *Cancer Control*, 2007, **14**, 295.
22 K. Sokolov, M. Follen, J. Aaron, I. Pavlova, A. Malpica, R. Lotan and R. Richards-Kortum, *Cancer Res.*, 2003, **63**, 1999.
23 I. H. El-Sayed, X. Huang and M. A. El-Sayed, *Cancer Lett.*, 2006, **239**, 129.
24 G. Han, P. Ghosh and V. M. Rotello, *Multi-functional gold nanoparticles for drug delivery,* 2007, Vol. 620, p. 48; C. M. Cobley, L. Au, J. Chen and Y. Xia, *Expert Opin. Drug Delivery*, 2010, **7**, 577
25 S. Bhattacharyya, R. Bhattacharya, S. Curley, M. A. McNiven and P. Mukherjee, *Proc. Natl. Acad. Sci. U. S. A.*, 2010, **107**, 14541.
26 N. Moreau, C. Michiels, B. Masereel, O. Feron, B. Gallez, T. Vander Borght and S. Lucas, *Plasma Process. Polym.*, 2009, **6**, S888.
27 J. Harding and B. Burtness, *Drugs Today*, 2005, **41**, 107.
28 E. J. Westover, D. F. Covey, H. L. Brockman, R. E. Brown and L. J. Pike, *J. Biol. Chem.*, 2003, **278**, 51125.
29 G. A. M. S. Van Dongen, G. W. M. Visser, M. N. Lub-De Hooge, E. G. De Vries and L. R. Perk, *Oncologist*, 2007, **12**, 1379.

